Trafficking defects in *WASH*-knockout fibroblasts originate from collapsed endosomal and lysosomal networks

Timothy S. Gomez[a,b], Jacquelyn A. Gorman[a], Amaia Artal-Martinez de Narvajas[b], Alexander O. Koenig[b], and Daniel D. Billadeau[a,b]

[a]Department of Immunology, Division of Oncology Research, and Schulze Center for Novel Therapeutics, and [b]College of Medicine, Mayo Clinic, Rochester, MN 55905

ABSTRACT **The Arp2/3-activator Wiskott–Aldrich syndrome protein and Scar homologue (WASH) is suggested to regulate actin-dependent membrane scission during endosomal sorting, but its cellular roles have not been fully elucidated. To investigate WASH function, we generated tamoxifen-inducible *WASH*-knockout mouse embryonic fibroblasts (WASHout MEFs). Of interest, although EEA1$^+$ endosomes were enlarged, collapsed, and devoid of filamentous-actin and Arp2/3 in WASHout MEFs, we did not observe elongated membrane tubules emanating from these disorganized endomembranes. However, collapsed WASHout endosomes harbored segregated subdomains, containing either retromer cargo recognition complex–associated proteins or EEA1. In addition, we observed global collapse of LAMP1$^+$ lysosomes, with some lysosomal membrane domains associated with endosomes. Both epidermal growth factor receptor (EGFR) and transferrin receptor (TfnR) exhibited changes in steady-state cellular localization. EGFR was directed to the lysosomal compartment and exhibited reduced basal levels in WASHout MEFs. However, although TfnR was accumulated with collapsed endosomes, it recycled normally. Moreover, EGF stimulation led to efficient EGFR degradation within enlarged lysosomal structures. These results are consistent with the idea that discrete receptors differentially traffic via WASH-dependent and WASH-independent mechanisms and demonstrate that WASH-mediated F-actin is requisite for the integrity of both endosomal and lysosomal networks in mammalian cells.**

Monitoring Editor
Judith Klumperman
University Medical Centre
Utrecht

Received: Feb 10, 2012
Revised: Jun 11, 2012
Accepted: Jun 15, 2012

INTRODUCTION

The Wiskott–Aldrich syndrome protein (WASP) family of nucleation-promoting factors stimulate filamentous (F)-actin polymerization through activation of the ubiquitous actin-related protein 2/3 (Arp2/3) complex (Goley and Welch, 2006; Takenawa and Suetsugu, 2007; Rottner *et al.*, 2010). The WASP family has emerged as essential regulators of several actin-dependent cellular processes, especially those involving the integration of the cytoskeleton with membrane dynamics. A highly conserved member of this WASP family, Wiskott–Aldrich syndrome protein and Scar homologue (WASH; Linardopoulou *et al.*, 2007), was recently demonstrated to be a unique regulator of F-actin–mediated endosomal trafficking events in mammalian cells (Derivery *et al.*, 2009; Gomez and Billadeau, 2009). However, little is known about how WASH-mediated F-actin networks function in the regulation of endosomal structure, sorting, and trafficking.

Functionally, several studies indicated that mammalian WASH specifically has a role at early endosomes and recycling endosomes. Use of small interfering RNA (siRNA) against WASH (siWASH) showed that WASH was essential for efficient transferrin receptor (TfnR) recycling, with WASH knockdown leading to exaggerated tubulation of the endosomal recycling compartment upon transferrin

This article was published online ahead of print in MBoC in Press (http://www.molbiolcell.org/cgi/doi/10.1091/mbc.E12-02-0101) on June 20, 2012.

Address correspondence to: Daniel D. Billadeau (billadeau.daniel@mayo.edu), Timothy S. Gomez (gomez.timothy@mayo.edu).

Abbreviations used: Arp2/3, actin-related protein 2/3; CSC, cargo sorting complex; EEA1, early endosomal–associated protein 1; EGFR, epidermal growth factor receptor; ER-Cre, estrogen receptor-Cre recombinase fusion; GFP, green fluorescent protein; LAMP1, lysosomal–associated membrane protein 1; MEF, mouse embryonic fibroblast; 4-OHT, 4-hydroxy tamoxifen; SHRC, WASH regulatory complex; SNX, sorting nexin; TfnR, transferrin receptor; VPS35, vacuolar protein sorting 35; WASH, Wiskott–Aldrich syndrome protein and SCAR homologue.

labeling (Derivery *et al.*, 2009). Although this recycling defect was confirmed by one study (Zech *et al.*, 2011), another study showed normal TfnR recycling using siWASH (Duleh and Welch, 2010). We found that retromer-mediated retrograde trafficking of the cation-independent mannose-6-phosphate receptor was defective, with WASH depletion resulting in the formation of aberrant, retromer-rich tubules (Gomez and Billadeau, 2009). Because exaggerated endosomal membrane tubulation was observed in WASH-suppressed cells, it was hypothesized that WASH regulated actin-dependent vesicle scission events (Derivery *et al.*, 2009; Gomez and Billadeau, 2009).

WASH knockdown was later suggested to delay trafficking of the epidermal growth factor receptor (EGFR) from endosomes to LAMP1$^+$ lysosomes (Duleh and Welch, 2010), although we previously showed that EGF-stimulated EGFR degradation proceeded normally in WASH-suppressed cells (Gomez and Billadeau, 2009). In addition, WASH was recently shown to regulate α5β1 integrin recycling, with α5β1 integrin aberrantly accumulating within a prelysosomal compartment in WASH-suppressed ovarian cancer cells (Zech *et al.*, 2011). Although these studies collectively suggest that WASH plays a role in several receptor-trafficking systems, it is unknown whether WASH activity is requisite for receptor trafficking from endosomes or some receptors traffic independent of WASH function.

Finally, we and others have identified that WASH functions at endosomes within a larger complex known as the WASH regulatory complex (SHRC), which includes FAM21, SWIP, strumpellin, and CCDC53 (Derivery *et al.*, 2009; Gomez and Billadeau, 2009; Jia *et al.*, 2010). The actin-capping protein heterodimer CapZα/β also associates with the SHRC through an interaction with FAM21 (Hernandez-Valladares *et al.*, 2010; Jia *et al.*, 2010). In addition, FAM21 regulates endosomal localization of the mammalian WASH complex via interaction with retromer cargo selection complex (CSC) component VPS35 (Harbour *et al.*, 2012; Jia *et al.*, 2012). Thus current knowledge suggests that mammalian WASH exists in a complex that is recruited to retromer-rich subdomains, where it functions to facilitate retromer-dependent sorting through actin-dependent membrane scission.

In addition to studies of mammalian WASH using siRNA, disruption of the *WASH* gene has been reported in *Drosophila* and *Dictyostelium*. *WASH* was shown to be essential for development through the larval stage in *Drosophila* (Linardopoulou *et al.*, 2007), whereas disruption of *Dictyostelium WASH* led to a defect in exocytosis of indigestible material due to inefficient sorting of V-ATPase during lysosomal neutralization (Carnell *et al.*, 2011). Of interest, a similar role for WASH complex function in the lysosomal compartment has not been described in mammalian cells. Moreover, a mammalian knockout of *WASH* has not been characterized.

Despite all of these recent findings, the role of WASH in endosome dynamics and receptor trafficking remains incompletely understood. Although several groups have made progress in defining the role of mammalian WASH in endosomal sorting using siRNA, this technology allows for partial phenotypes due to incomplete depletion. To analyze the cellular phenotype associated with loss of mammalian WASH, we generated *WASH*-knockout (WASHout) mouse embryonic fibroblasts (MEFs). Our initial characterization of these WASHout MEFs demonstrates that WASH-mediated F-actin is requisite for the integrity of both endosomal and lysosomal networks in mammalian cells. In addition, although EGFR is basally directed to lysosomes and degraded in WASHout fibroblasts, TfnR levels remain constant in the absence of WASH. These results suggest that EGFR is a WASH-dependent cargo under basal conditions and are consistent with the idea that discrete receptors differentially traffic via WASH-dependent and WASH-independent mechanisms.

RESULTS

WASH-knockout fibroblasts are viable and display diminished SHRC expression

To delineate the cellular role of WASH, we created mice that have the second exon of *WASH* flanked by *Lox*P sites ("floxed"; Supplemental Figure S1). These conditional *WASH*-knockout mice were first bred to protamine-Cre mice to establish total *WASH*-knockout animals, which we found to be embryonic lethal before embryonic day 7.5 (E7.5; data not shown). Therefore we generated *WASH*$^{-/-}$ mouse embryonic fibroblasts (WASHout MEFs) as a model to study WASH function. *WASH*$^{+/flox}$ mice were interbred with *WASH*$^{+/flox}$ mice that also expressed estrogen receptor-Cre recombinase fusion (*WASH*$^{+/flox}$/ER-Cre$^+$). MEFs isolated from *WASH*$^{flox/flox}$/ER-Cre$^+$ offspring were subsequently exposed to 4-hydroxy tamoxifen (4-OHT) to generate WASHout MEFs. Cre recombinase activity resulted in efficient depletion of WASH, as shown by immunoblotting and immunofluorescence for mWASH (Figure 1, A–D). In addition, flow cytometry for mWASH indicated efficient deletion of *WASH* in the 4-OHT–treated population (Supplemental Figure S1F). In contrast, 4-OHT–treated *WASH*$^{+/+}$ ER-Cre$^+$ control fibroblasts did not lose WASH expression (Figure 1A).

We previously demonstrated that shRNA against WASH destabilized CCDC53, whereas levels of the other SHRC components were only mildly affected (Jia *et al.*, 2010). However, in WASHout MEFs, we found that all SHRC components were substantially reduced in the absence of WASH (Figure 1A), conclusively illustrating that stability of the entire SHRC is WASH dependent. However, SHRC-associated CapZ appears stable without WASH (Figure 1A). In addition, although we found that residual FAM21, SWIP, and strumpellin remained associated in the absence of WASH, the small amount of remaining CCDC53 did not interact with other SHRC components in WASHout MEFs (Figure 1B), which is in agreement with our suggested model of SHRC assembly (Chen *et al.*, 2010; Jia *et al.*, 2010). In addition, CapZ remained associated with FAM21 in the absence of WASH, consistent with the known CapZ-interacting motif in the FAM21 C-terminus (Figure 1B). Thus we have generated inducible *WASHout* MEFs, permitting in-depth study of the cellular role of mammalian WASH.

WASHout fibroblasts display a collapsed endosomal network and a complete absence of endosomal F-actin

Because short hairpin RNA (shRNA)–mediated depletion of WASH led to diminished endosomal F-actin accumulation and exaggerated endosomal tubulation due to potential scission defects (Derivery *et al.*, 2009; Gomez and Billadeau, 2009), we first examined early endosomes in WASHout MEFs. In the absence of WASH, the EEA1$^+$ endosomal network exhibited a dramatically altered appearance under normal growth conditions (Figure 1D). Endosomes did not exhibit any aberrant tubular structures but instead collapsed to the perinuclear region. In addition, whereas endosomes in the *WASH*$^{flox/flox}$ fibroblasts were clearly decorated with F-actin, the collapsed endosomal network of WASHout MEFs was completely devoid of F-actin (Figure 1, E–H). These WASHout endosomes exhibited various morphologies, including clusters (Figure 1H), vacuolar-like structures (Figure 1I), and what resembled short, actin-free sorting tubules (Figure 1J). In addition, endosomal-associated Arp2/3-rich puncta were absent in WASHout MEFs (Figure 1, K and L). Reconstitution of WASHout MEFs with wild-type green fluorescent protein (GFP)–mWASH rescued loss of endosomal

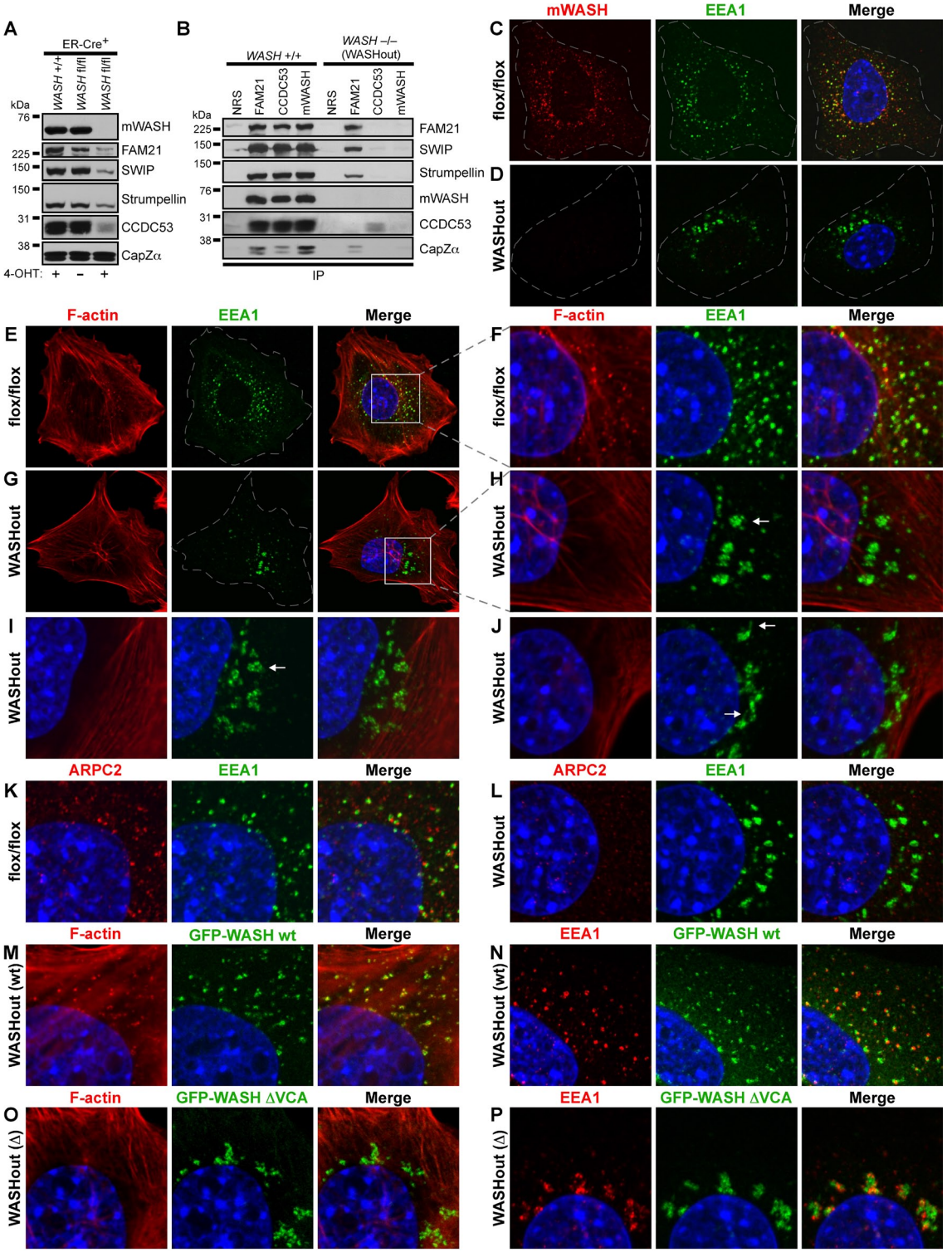

FIGURE 1: WASH-knockout MEFs display reduced SHRC expression and collapsed endosomes devoid of F-actin. (A) *WASH*$^{flox/flox}$/ER-Cre^{+} MEFs were left untreated or treated with 4-OHT to induce *WASH* knockout. Control *WASH*$^{+/+}$/ER-Cre^{+} MEFs were also treated with 4-OHT. Lysates were immunoblotted as indicated. (B) Immunoprecipitations were performed using the indicated antibodies from lysates of either 4-OHT–induced *WASH*$^{-/-}$ (WASHout) MEFs or *WASH*$^{+/+}$ control MEFs. (C, D) *WASH*$^{flox/flox}$ and WASHout MEFs were analyzed by immunofluorescence for mWASH (red) and EEA1 (green). (E-J) *WASH*$^{flox/flox}$ and WASHout MEFs were stained with rhodamine–phalloidin for F-actin (red) and with anti-EEA1 (green). Arrows indicate distinct endosomal morphologies. (F, H) Insets from E and G as indicated. (K, L) *WASH*$^{flox/flox}$ and WASHout MEFs were stained with anti-EEA1 (green) and anti-ARPC2 (red). (M, N) WASHout MEFs reconstituted with wild-type GFP-WASH were costained with rhodamine–phalloidin (red) or with anti-EEA1 (red), respectively. (O, P) WASHout MEFs reconstituted with GFP-WASH ΔVCA were costained with rhodamine–phalloidin (red) or with anti-EEA1 (red), respectively. (C–P) The nucleus is shown via Hoechst staining (blue).

F-actin and endosomal collapse, indicating that the endosomal collapse was a direct result of WASH deletion (Supplemental Figure S2A and Figure 1, M and N). However, complementation, using GFP-mWASH ΔVCA, lacking the ability to interact with G-actin and the Arp2/3 complex, did not rescue the phenotype, confirming that loss of WASH-mediated F-actin polymerization specifically led to the endosomal collapse (Supplemental Figure S2A and Figure 1, O–P). Of interest, GFP-mWASH-ΔVCA localized near collapsed EEA1$^+$ endosomes but did not display strong overlap with the EEA1 marker (colocalization coefficient, 0.32 ± 0.08; Figure 1P). Moreover, these endosomal morphological changes in WASHout MEFs did not result from altered microtubule structure (Supplemental Figure S2, B and C), or global membrane-trafficking defects, since the clathrin-rich compartment and Golgi morphology were unaffected (Supplemental Figure S2, D–G).

We next stained control and WASHout MEFs with various endosomal-associated proteins to determine the step in the endosomal maturation process at which this collapse occurred. The pleckstrin homology domain–containing protein APPL1 designates early endocytic intermediates before PI3P conversion and EEA1 recruitment (Zoncu *et al.*, 2009). APPL1-stained vesicles appeared along the cell periphery in both control and WASHout MEFs, indicating that these early endocytic events were occurring normally (Supplemental Figure S3, A and B). The FYVE domain–containing protein RUFY1, which is involved in transferrin recycling (Yamamoto *et al.*, 2010), exists on a subset of EEA1$^+$ endosomes in control cells (Supplemental Figure S3C). In WASHout MEFs, RUFY1 cocollapsed along with the EEA1-stained endosomal network but did not overlay entirely with EEA1 staining (colocalization coefficient, 0.39 ± 0.09; Supplemental Figure S3D). HRS, which has multiple functions during endosomal maturation, from initial clathrin recruitment to receptor degradation events (Raiborg *et al.*, 2001, 2002), was associated with early EEA1–negative endocytic vesicles, as well as with EEA1$^+$ endosomes in control MEFs (Supplemental Figure S3E). Of interest, in WASHout MEFs, HRS staining demonstrated a clear demarcation between normal proximal endocytic events and the EEA1$^+$ collapse in the endosomal network (Supplemental Figure S3F). In sum, while we did not observe abnormal tubular structures while analyzing these endocytic markers in WASHout MEFs, we found that that the endosomal network dramatically collapsed in the absence of WASH. Moreover, this collapse seemed to occur at the stage of APPL1$^+$-to-EEA1$^+$ endosomal conversion (Zoncu *et al.*, 2009).

Retromer and SHRC components designate an EEA1-negative subdomain of collapsed endosomes in WASHout fibroblasts

We next examined whether the residual SHRC components localized to collapsed endosomes in WASHout MEFs. FAM21 localized near endosomes in the absence of WASH (Figure 2, A and B), which is consistent with its role in endosomal targeting of the entire SHRC (Gomez and Billadeau, 2009). Although FAM21 staining resembled the collapsed EEA1$^+$ structures, FAM21 marked a discrete and mostly EEA1-negative subdomain of the collapsed endosomes (colocalization coefficient, 0.31 ± 0.09; Figure 2B), which was similar to that observed for WASH-ΔVCA localization seen in Figure 1P. These FAM21 subdomains appeared contiguous with EEA1$^+$ membranes in confocal slices and displayed some short tubules, which were also distinct from EEA1$^+$ tubules (Figure 2C). This suggests that WASHout endosomes do not display global domain mixing during collapse but maintain segregated organization.

Given that the retromer CSC component VPS35 was recently shown to recruit FAM21 to endosomes (Harbour *et al.*, 2012; Jia *et al.*, 2012), we next examined VPS35 localization in WASHout fibroblasts. Similar to FAM21, VPS35 accumulation with EEA1 was distinct in WASHout MEFs (colocalization coefficient, 0.32 ± 0.08; Figure 2, D and E). However, double staining of FAM21 and VPS35 indicated that indeed these proteins colocalized in the absence of WASH (colocalization coefficient, 0.93 ± 0.04), demarcating the same collapsed endosomal compartment (Figure 2, F and G). The Rab-GAP TBC1D5, which was also suggested to be retromer recruited (Harbour et al., 2010), similarly costained with VPS35 in WASHout MEFs (colocalization coefficient, 0.83 ± 0.05; Supplemental Figure S4). Moreover, the SHRC component SWIP accumulated with VPS35 in WASHout fibroblasts (colocalization coefficient, 0.9 1± 0.02; Figure 2, H and I), whereas CCDC53, which localizes to endosomes in control cells overlaying with VPS35 staining, did not localize with either EEA1 or VPS35 in WASHout MEFs (Supplemental Figure S5, A–D). This is consistent with CCDC53 dissociation from other SHRC members without WASH (Figure 1B). The discrete overlap of VPS35, FAM21, SWIP, and TBC1D5 suggested that WASHout endosomes are partly composed of defined EEA1$^+$ and retromer$^+$ subdomains.

Sorting nexin proteins (SNX1/2/5/6) also regulate retromer-dependent sorting events (Cullen, 2008), so we next tested whether SNXs localized to the retromer subdomain of WASHout endosomes. Of interest, SNX1 staining was more confined to the EEA1$^+$ region of collapsed endosomes (colocalization coefficient, 0.78 ± 0.04) and displayed less overlap VPS35 (colocalization coefficient, 0.47 ± 0.08; Supplemental Figure S6, A–C). In addition, SNX6 similarly displayed EEA1 costaining (colocalization coefficient, 0.79 ± 0.02), as well as localization to the *cis*-Golgi (Supplemental Figure S6, D–F). Thus these retromer-related SNX proteins did not localize strongly to the retromer-enriched subdomain of WASHout endosomes. Taken together, these data demonstrate that collapsed endosomes in WASHout MEFs retain distinct segregation of EEA1$^+$ and retromer CSC-rich subdomains.

Lysosomes globally collapse in WASHout fibroblasts

Given the collapsed phenotype of the endosomal compartment in WASHout MEFs and the requisite dependence of lysosomes on endosomal function, we next examined lysosomal structures in the WASHout cells. We stained WASHout fibroblasts with RAB7 and LAMP1, which are markers of vesicular trafficking steps associated with late endosomes and lysosomes. We observed strong overlap of these markers on scattered lysosomes in control cells (colocalization coefficient, 0.82 ± 0.04; Figure 3A). However, upon *WASH* knockout, lysosomes dramatically collapsed (Figure 3B), displaying common morphologies, including large, vacuolated structures, thin tubules, and elongated/bundled lysosomal tracks (Figure 3C). Moreover, consistent with the fact that a degree of proximity could be observed between lysosomes and endosomes in control cells (Figure 3D), some of the altered WASHout lysosomes were collapsed to areas adjacent to EEA1$^+$ structures (Figure 3E). However, the EEA1-bright domains remained mostly segregated from the LAMP1-bright regions (colocalization coefficient, 0.19 ± 0.06). The retromer-rich section (VPS35$^+$) of WASHout endosomes demonstrated an intimate relationship with some of the collapsed LAMP1$^+$ lysosomes, although it was mostly segregated from the LAMP1-bright regions (colocalization coefficient, 0.32 ± 0.04; Figure 3, F and G). Consistent with VPS35 staining, FAM21 showed a similar connection with a subset of collapsed lysosomes (colocalization coefficient, 0.32 ± 0.03; Figure 3H).

To designate the relative positioning of collapsed endosomal domains with lysosomal structures in WASHout MEFs, we next triple

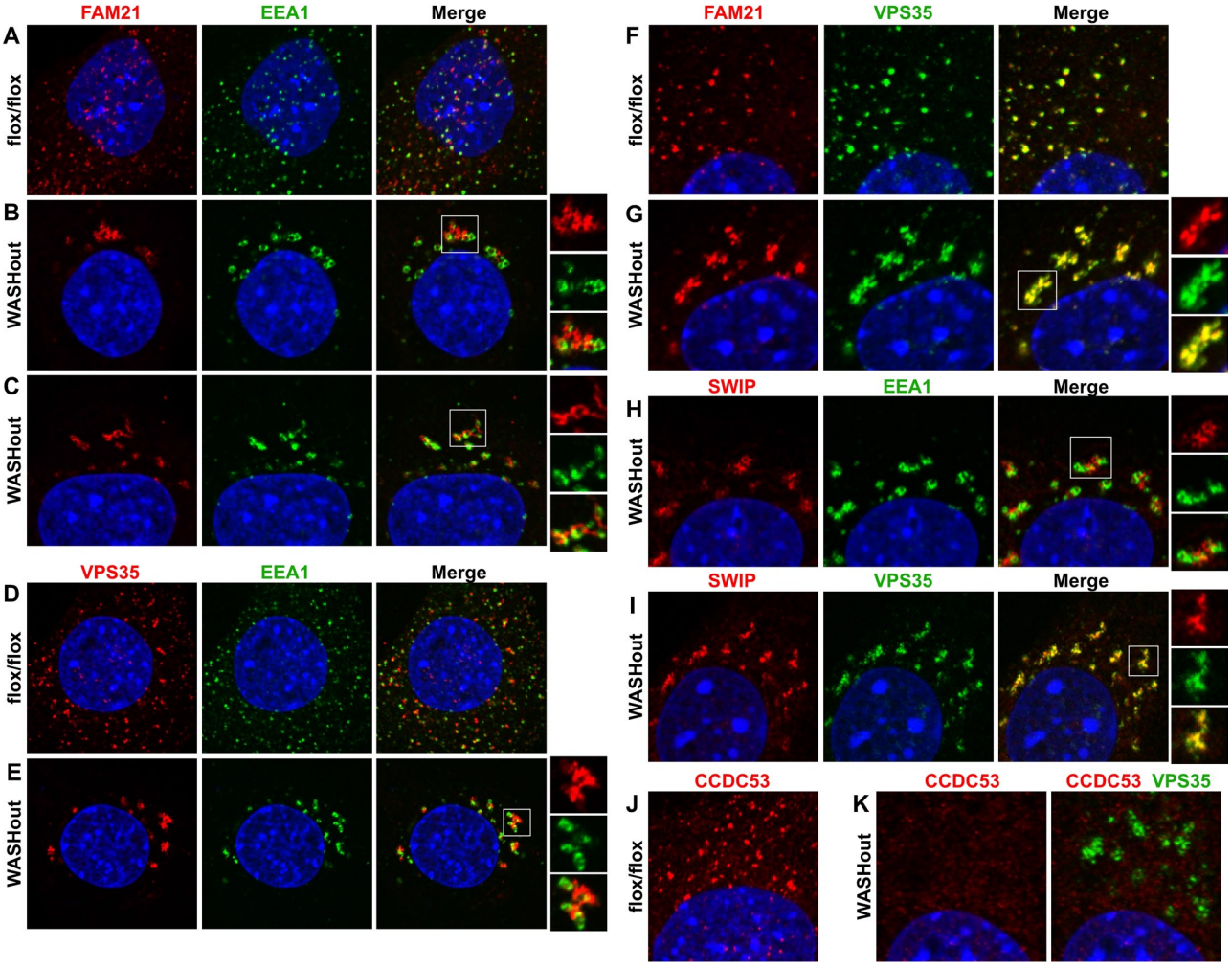

FIGURE 2: Collapsed endosomes in WASHout fibroblasts harbor distinct subdomains enriched in retromer CSC and SHRC components. *WASH*$^{flox/flox}$ and WASHout MEFs were analyzed by immunofluorescence as indicated. The nucleus is shown via Hoechst staining (blue).

stained cells with EEA1, FAM21 (to mark the retromer-rich compartment), and LAMP1. In control MEFs, FAM21 demonstrated clear punctate association with EEA1$^+$ endosomes, as expected (Figure 4A). In addition, we observed that FAM21$^+$/EEA1$^+$ endosomal structures were associated with some, but not all, of the LAMP1$^+$ puncta in control cells, likely representing the normal transitioning or communication occurring between these compartments (Figure 4A). This staining verified that these three markers (FAM21$^+$, EEA1$^+$, and LAMP1$^+$), although intimately related, represented mostly distinct regions on collapsed endomembranes in WASHout MEFs (Figure 4B). These data for the first time illustrate altered lysosomal morphology in WASH-deficient mammalian cells. Moreover, we demonstrate that a subset of collapsed WASHout lysosomes maintain close, yet distinct, association with enlarged endosomes in *WASH*-knockout MEFs.

Transferrin receptor is accumulated with collapsed endosomes in WASHout MEFs

It was previously shown that WASH-suppressed 3T3 cells formed elongated endosomal tubules upon loading with fluorescently labeled transferrin (Derivery *et al.*, 2009). However, whether WASH is required for TfnR recycling is controversial (Duleh and Welch, 2010). Because we did not observe similar tubular structures using several endosomal markers in the absence of WASH, we next analyzed AF555-transferrin uptake as a means to potentially visualize any aberrant tubulation occurring in WASHout MEFs. In control MEFs, we saw efficient transferrin uptake within many scattered WASH$^+$ endosomes (Figure 5A). However, in WASHout MEFs, internalized transferrin accumulated in enlarged perinuclear structures that did not appear under the same conditions in WASH-expressing MEFs (Figure 5A). Surprisingly, in WASHout MEFs we never observed the previously described tubular structures that were seen with siWASH and transferrin labeling.

Because internalized AF555-transferrin abnormally accumulated in WASHout MEFs, we next wanted to determine the localization of TfnR in the absence of WASH. Under normal growth conditions, TfnR in control MEFs was localized to many puncta dispersed throughout the cell, consistent with endosomal localization (Figure 5B). However, in WASHout MEFs, TfnR showed an accumulated pattern that mirrored the AF555-transferrin labeling in WASHout cells (compare Figure 5, A and B). On further analysis, we found that TfnR was partially localized with EEA1$^+$ collapsed endosomes in WASHout MEFs (colocalization coefficient, 0.39 ± 0.03; Figure 5C). Similarly, TfnR was adjacent to retromer CSC-enriched subdomains of

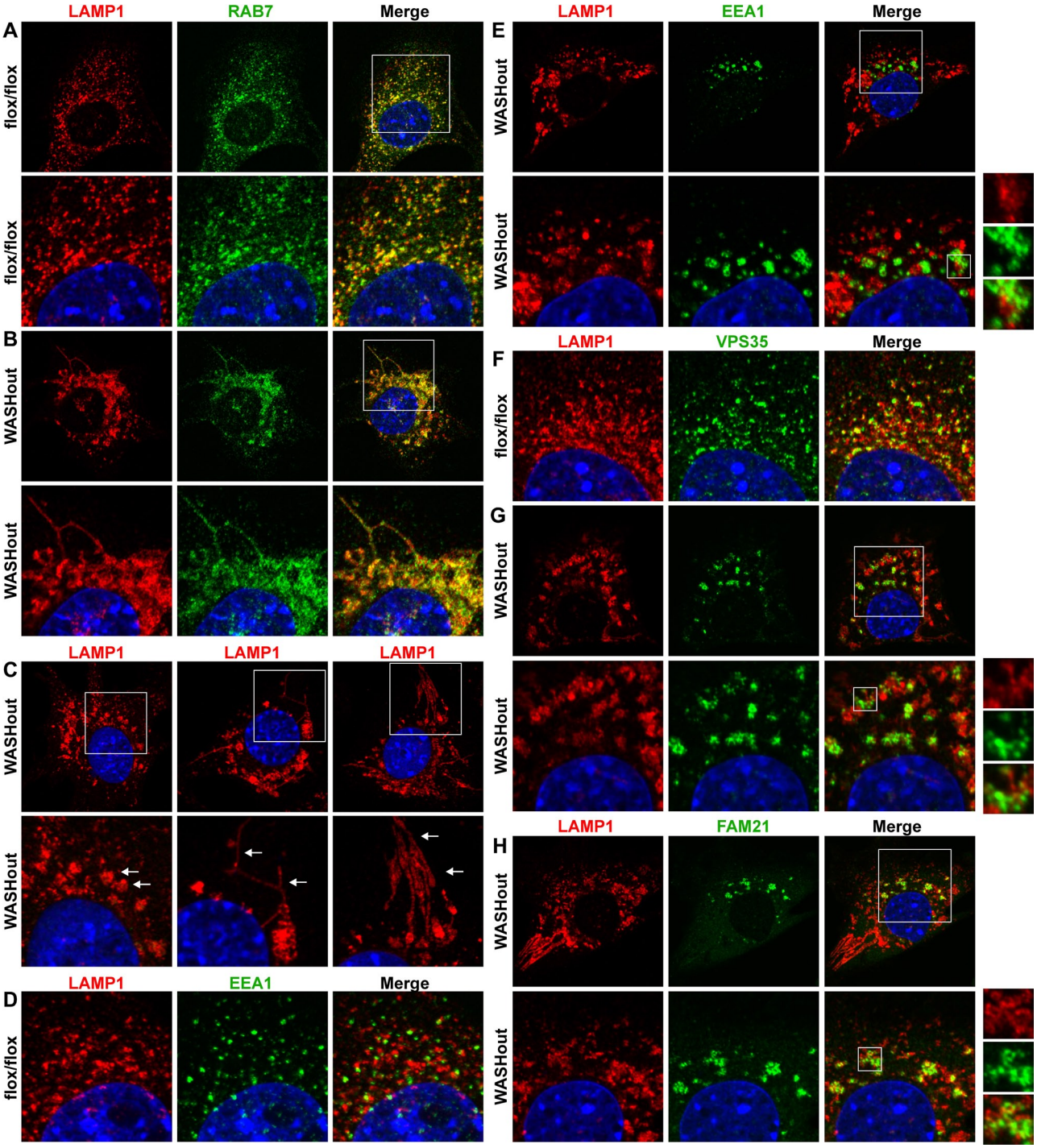

FIGURE 3: Lysosomes collapse in WASHout fibroblasts. *WASH*$^{flox/flox}$ and WASHout MEFs were analyzed by immunofluorescence as indicated. In C the arrows within the insets indicate distinct lysosomal morphologies. The nucleus is shown via Hoechst staining (blue).

WASHout endosomes, showing some overlap with FAM21 staining (colocalization coefficient, 0.39 ± 0.03; Figure 5D). In contrast, TfnR was less intimately associated with LAMP1$^+$ lysosomes in WASHout MEFs (colocalization coefficient, 0.29 ± 0.08; Figure 5E). Although TfnR seemed to be sequestered within WASHout endosomes, surface staining for TfnR indicated normal receptor levels compared with WASH-expressing MEFs (Figure 5F). In addition, total cellular levels of TfnR were unchanged in WASHout MEFs (Figure 5G), consistent with TfnR separation from lysosomes (Figure 5E).

To test whether TfnR trafficking was affected in WASHout MEFs, we used a flow cytometry–based assay to examine both uptake and recycling of TfnR using fluorescently labeled ligands. Initial uptake of AF488-Tfn was not significantly altered in WASHout MEFs when compared with control (AF488 up to 30 min; Figure 5H). In addition, TfnR recycling was unaffected, as observed by exchanging the AF488-Tfn–containing media with AF647-Tfn at the point of maximal AF488-Tfn loading (30 min), which resulted in unloading of AF488-Tfn and new accumulation of the AF647-Tfn via recycled

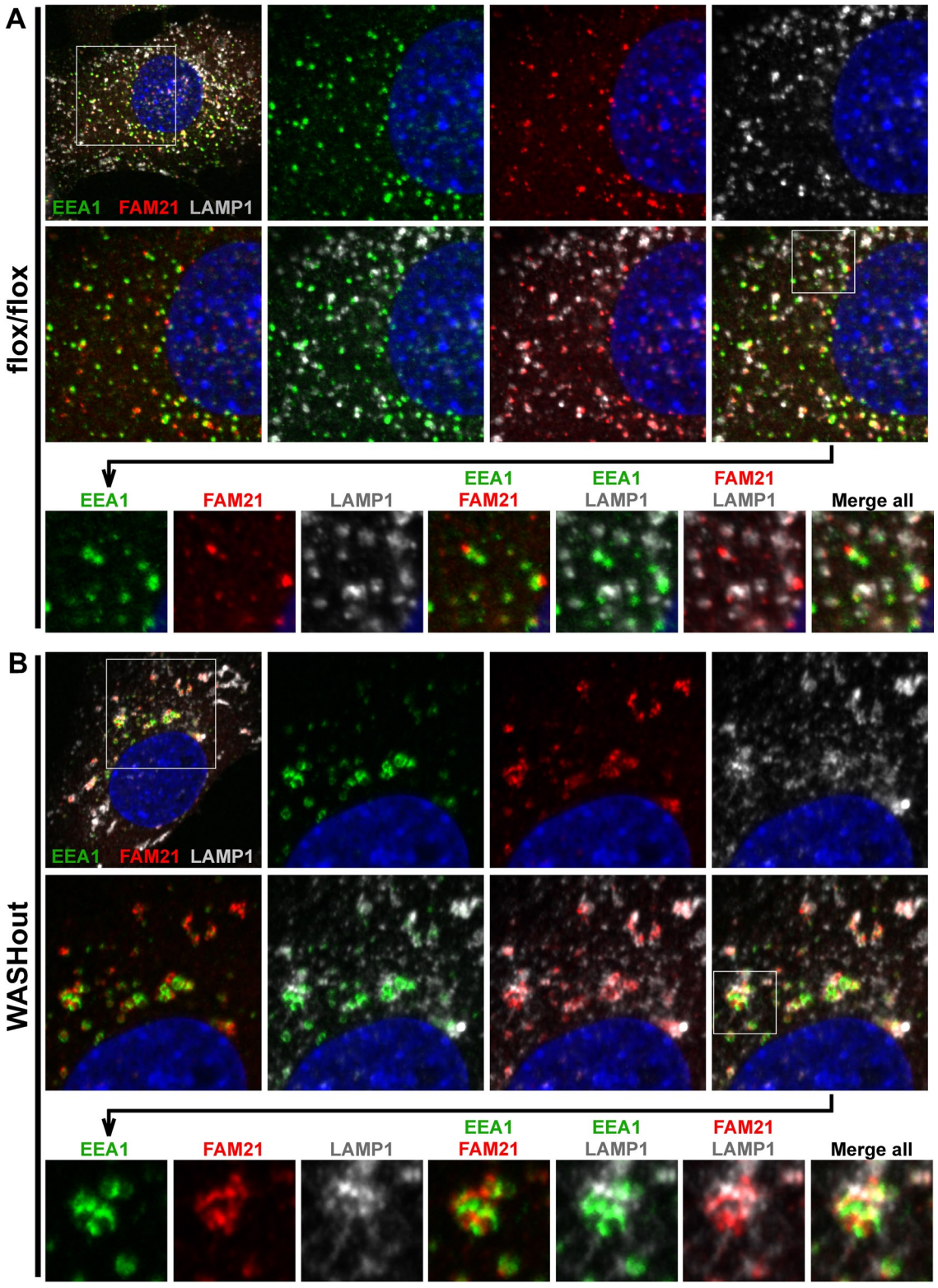

FIGURE 4: Collapsed EEA1$^+$, retromer-rich, and LAMP1$^+$ domains in WASHout MEFs remain distinct. *WASH*$^{flox/flox}$ and WASHout MEFs were analyzed by immunofluorescence as indicated. Sequential insets are displayed as indicated. The nucleus is shown via Hoechst staining (blue).

receptors (after 30 min; Figure 5H). In sum, we did not visualize aberrant tubular structures forming in transferrin-labeled WASHout MEFs, indicating that the WASHout phenotype is distinct from that observed with siRNA against WASH. Instead of being sequestered into long tubules in WASHout MEFs, TfnR was accumulated near collapsed endosomes. In addition, we found that TfnR recycling was unaffected in the absence of WASH, suggesting that WASH does not regulate the trafficking of this receptor.

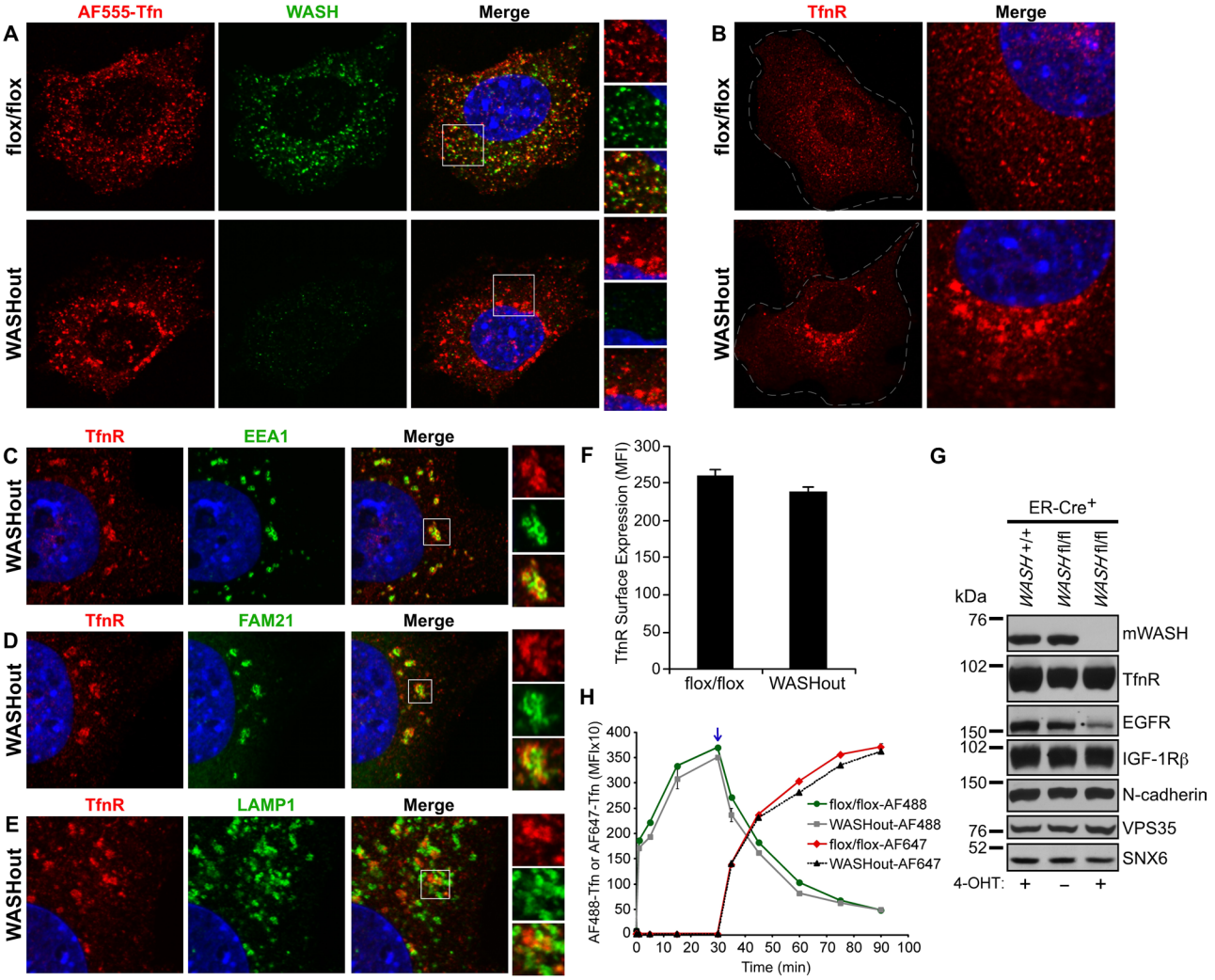

FIGURE 5: Transferrin receptor shows altered localization but normal levels in WASHout MEFs. (A–E) *WASH*$^{flox/flox}$ and WASHout MEFs were analyzed by immunofluorescence as indicated. The nucleus is shown via Hoechst staining (blue). (F) Transferrin receptor surface levels were analyzed by flow cytometry. (G) *WASH*$^{flox/flox}$/ER-Cre^{+} MEFs were left untreated or treated with 4-OHT. *WASH*$^{+/+}$/ER-Cre^{+} MEFs were also 4-OHT treated as a control. Lysates were immunoblotted as indicated. (H) *WASH*$^{flox/flox}$ and WASHout MEFs were analyzed by flow cytometry for uptake of AF488-Tfn (AF488 up to 30 min). AF488-Tfn was then exchanged with AF647-Tfn in order to analyze TfnR-mediated recycling of AF488-Tfn (AF488; after 30 min) and new accumulation of AF647-Tfn (AF647 after 30 min) via two-color flow-cytometric analysis. Blue arrow indicates point of AF488-Tfn and AF647-Tfn exchange.

WASH knockout leads to reduction of EGFR

During analysis of total TfnR levels in WASHout MEFs, we also examined other receptors as a way to gauge potential trafficking defects in WASHout MEFs. Of interest, we found that steady-state EGFR levels were significantly reduced in WASHout MEFs under normal growth conditions, whereas insulin like growth factor-1 (IGF-1) receptor β and N-cadherin levels remained constant (Figure 5G). We previously showed that stimulated EGFR localizes with WASH upon internalization and is efficiently degraded upon activation in WASH-suppressed cells (Gomez and Billadeau, 2009). However, with the use of siRNA toward WASH, a separate study suggested that EGFR trafficking to lysosomes was delayed (Duleh and Welch, 2010). Of importance, EGFR reduction in WASHout MEFs was not a result of 4-OHT treatment, as EGFR was stably diminished compared with control cells up to 2 wk after treatment (Figure 6A). Moreover, there was a concomitant decrease in EGFR surface levels upon loss of WASH (Figure 6B), and EGFR reduction was not secondary to a change in EGFR mRNA levels (Figure 6C).

Because EGFR levels were reduced in WASHout MEFs, we next examined whether EGFR-mediated signaling was affected. On EGF stimulation, EGFR was degraded with normal kinetics up to 1 h posttreatment in WASHout MEFs, after which kinetics was altered owing to complete degradation of the initially lower EGFR levels in *WASH*$^{-/-}$ MEFs (Figure 6, D and E). Consistent with lower basal EGFR levels, WASHout MEFs exhibited decreased EGF-stimulated activation of AKT, c-Raf, and ERK (Figure 6D). Of interest, the strength and duration of JNK phosphorylation was unaffected, which could indicate a decreased threshold for EGFR-mediated JNK activation (Figure 6D). Although it is possible that WASH directly regulates key receptor-mediated signaling pathways, IGF-stimulated WASHout MEFs did not exhibit similar defects in ERK activation (data not shown).

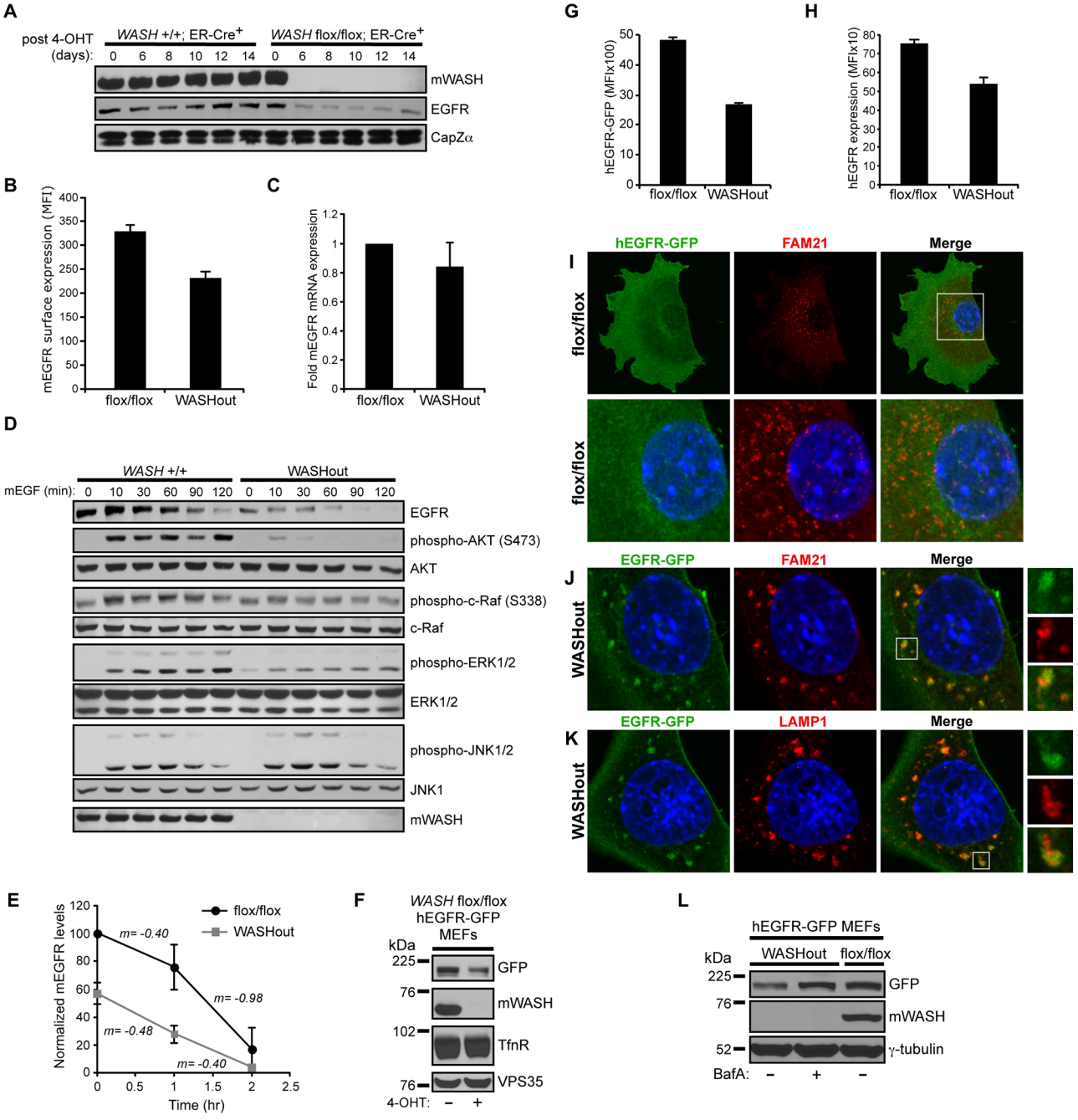

FIGURE 6: EGFR is reduced and localizes with lysosomes at steady state in WASHout MEFs. (A) Control *WASH*$^{+/+}$/ER-Cre^{+} and *WASH*$^{flox/flox}$/ER-Cre^{+} MEFs were treated with 4-OHT over time. Lysates were immunoblotted as indicated. (B) Basal mEGFR surface levels were analyzed by flow cytometry. (C) Basal mEGFR mRNA levels were measured with quantitative reverse transcriptase PCR. (D) Control and WASHout MEFs were treated with mEGF over time, and lysates were immunoblotted as indicated. (E) EGFR degradation was quantified from immunoblots via densitometry from three independent experiments, and the slope (*m*) is indicated between time points. (F) *WASH*$^{flox/flox}$/ER-Cre^{+}/hEGFR-GFP–expressing MEFs were treated or not treated with 4-OHT, and lysates were immunoblotted as indicated. (G, H) Total hEGFR-GFP expression and surface hEGFR levels were measured by flow cytometry using hEGFR-GFP–expressing *WASH*$^{flox/flox}$ and WASHout MEFs. (I–K) hEGFR-GFP–expressing *WASH*$^{flox/flox}$ and WASHout MEFs were analyzed by immunofluorescence as indicated. The nucleus is shown via Hoechst staining (blue). (L) hEGFR-GFP–expressing WASHout MEFs were left untreated or treated with 400 nM bafilomycin A for 20 h and analyzed by immunoblot as indicated.

To study EGFR trafficking and degradation in the absence of WASH, we generated a hEGFR-GFP–expressing *WASH*$^{flox/flox}$/ER-Cre^{+} fibroblast line. When these cells were treated with 4-OHT to delete *WASH*, hEGFR-GFP levels were reduced in a similar manner to that of the endogenous receptor (Figure 6F). This is consistent with an EGFR-trafficking defect leading to receptor loss in WASHout MEFs because hEGFR-GFP is driven by a separate promoter and yet is still affected. In fact, total and surface hEGFR-GFP reduction could be seen by flow cytometry (Figure 6, G and H). Under normal growth conditions, the localization of hEGFR-GFP in WASH-expressing

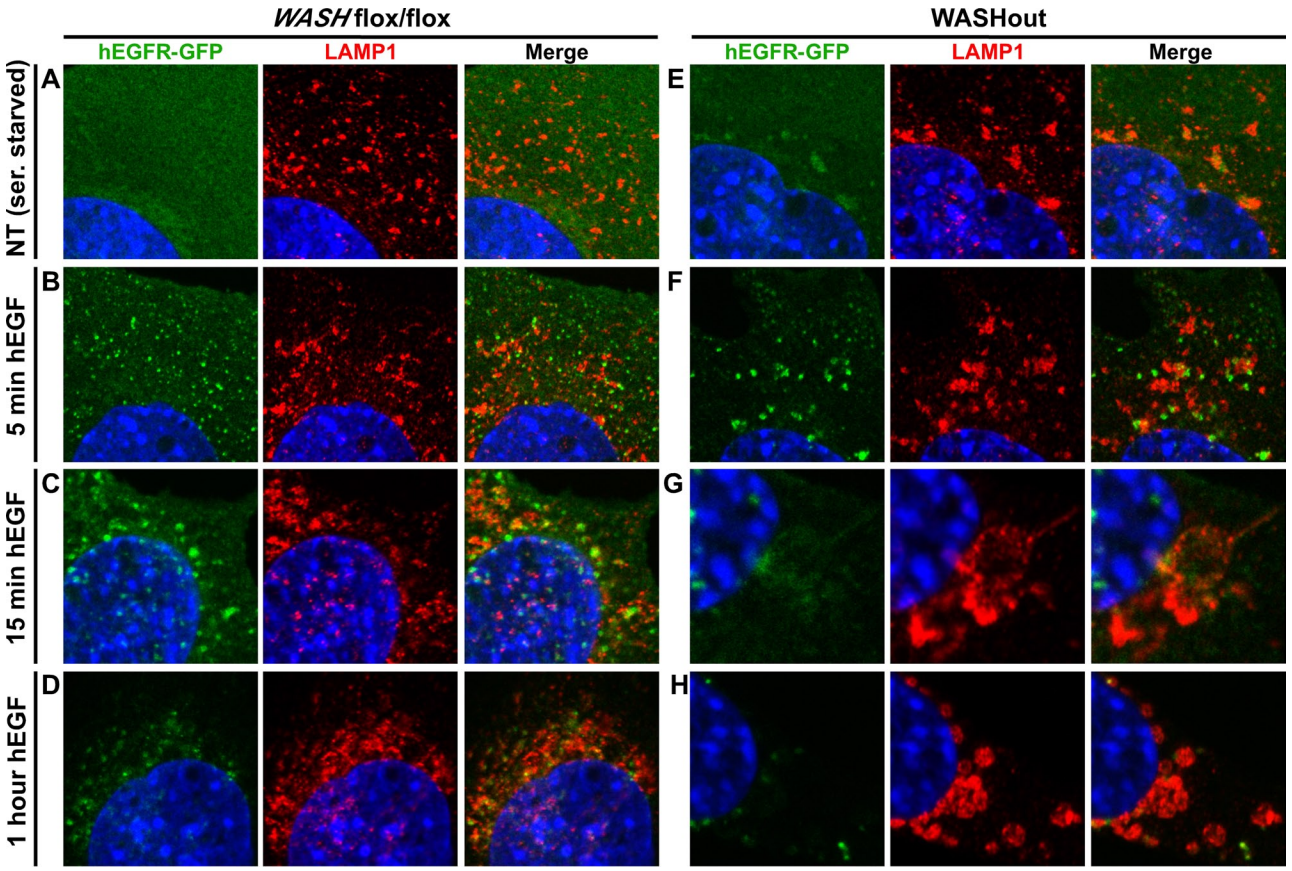

FIGURE 7: EGFR is degraded within enlarged lysosomal structures upon activation in WASHout MEFs. hEGFR-GFP–expressing *WASH*$^{flox/flox}$ and WASHout MEFs were analyzed by immunofluorescence after either serum starvation or stimulation with hEGF over the indicated time course. The nucleus is shown via Hoechst staining (blue).

control cells was diffuse and not obviously localized with endosomes or lysosomes (Figure 6I and data not shown). However, hEGFR-GFP in WASHout MEFs was accumulated with collapsed endomembrane structures, localizing with FAM21-bright subdomains of endosomes (colocalization coefficient, 0.68 ± 0.08; Figure 6J). In fact, hEGFR-GFP showed even stronger overlap with WASHout lysosomes (colocalization coefficient, 0.89 ± 0.07; Figure 6K). In addition, treating hEGFR-GFP–expressing WASHout cells with the V-ATPase inhibitor bafilomycin A rescued the decrease in EGFR levels (Figure 6L), confirming that EGFR was shunted to degradation in lysosomes in the absence of WASH. In sum, total and surface levels of EGFR are lower in the absence of WASH, leading to defects in signaling, and under normal growth conditions EGFR localized with collapsed lysosomes and was degraded basally and following EGF stimulation.

Stimulated EGFR degradation occurs within enlarged lysosomal structures in WASHout MEFs

The collapsed lysosomes of WASHout MEFs appeared to be fully functional, as EGFR was efficiently degraded upon stimulation (Figure 6D). This, coupled with the fact that EGFR displayed steady-state accumulation with lysosomes and showed reduced basal levels in WASHout MEFs, suggested an EGFR-trafficking defect in the absence of WASH. Thus we next analyzed the kinetics of EGF-mediated hEGFR-GFP internalization. Using rhodamine-hEGF, we could easily visualize EGF/EGFR complexes internalizing into control cells. As expected, small EGF/EGFR-rich vesicles appeared in control cells within minutes of stimulation and later fused into larger endosomal structures. EGFR-GFP was ultimately degraded in lysosomes, resulting in loss of signal (Supplemental Figure S7). Of interest, even under conditions of serum starvation, WASHout MEFs exhibited basal accumulation of EGFR-GFP on endomembranes (Supplemental Figure S7). On stimulation, EGFR-GFP was internalized into the enlarged endosomes of WASHout MEFs. Although fewer EGFR-rich puncta were observed, those that appeared were larger compared with control cells and remained enlarged even at later time points during degradation (Supplemental Figure S7).

We next followed EGF-stimulated EGFR-GFP in relation to lysosomes in control and WASHout MEFs. Again, in serum-starved WASHout cells, it was clear the EGFR-GFP was basally accumulated with collapsed lysosomes in contrast to control cells (Figure 7, A and E). Stimulated WASH-expressing control cells exhibited aggregation of lysosomes toward the perinuclear region throughout activation, and EGFR-GFP became more associated with these lysosomes over time (Figure 7, A–D, and Supplemental Figure S8). Of interest, the collapsed lysosomes of WASHout MEFs also aggregated over time, but unlike control cells, they fused together to form large, vacuolar structures that contained residual EGFR-GFP signal (Figure 7, E–G, and Supplemental Figure S8). It is striking that these round lysosomal structures commonly became denser at the end of the EGF-stimulated time course and were morphologically reminiscent of autophagosomes (Figure 7H and Supplemental Figure S8). By adjusting the laser intensity, we could observe dim EGFR-GFP signal within these lysosomal structures, which suggested that EGFR was degraded within these activated WASHout lysosomes (data not

shown). Taken together, WASHout fibroblasts produced enlarged lysosomal structures during EGF stimulation that mediated efficient EGFR degradation.

DISCUSSION

Here we characterized the cellular phenotype associated with mammalian *WASH* knockout. Endosomes were enlarged and collapsed in the absence of WASH-mediated F-actin. However, we did not observe exaggerated endosomal membrane tubulation, which we had anticipated in context of the current model of WASH function in endosomal scission based on siRNA studies (Derivery *et al.*, 2009; Gomez and Billadeau, 2009). Moreover, we found that collapsed WASHout endosomes did not exhibit global subdomain mixing. We also demonstrated a role for mammalian WASH in maintaining the integrity of the lysosomal compartment, which also collapsed in the absence of WASH. In addition, EGFR was directed to this collapsed lysosomal compartment and exhibited reduced basal levels in WASHout MEFs, whereas steady-state TfnR levels were unaffected.

In line with previous studies using siWASH, WASH knockout resulted in altered endosomal morphology (Derivery *et al.*, 2009; Gomez and Billadeau, 2009; Duleh and Welch, 2010). However, WASH knockout had a more severe general effect on endosomes, which dramatically enlarged, collapsed, and changed shape without WASH. Although the degree of endosomal compartment collapse that we observed was surprising, similar effects on endosomes have been described using drugs that globally depolymerize F-actin (Duleh and Welch, 2010). This, and the fact that WASHout endosomes are devoid of F-actin, is consistent with the idea that WASH is principally responsible for generating the endosomal F-actin network. In line with this, reexpression of wild-type WASH rescued the collapsed endosomal network, whereas the ΔVCA mutant did not. Endosomal enlargement and collapse could simply be a byproduct of inefficient sorting away from endosomes without WASH. Alternatively, collapse could result from loss of physical barriers normally imposed by F-actin coats on individual endosomes, leading to an increase in fusion events or defects in seclusion.

In addition, the absence of previously described tubulation events in WASH-knockout cells suggested a more severe defect associated with complete loss of WASH. However, our results do not preclude the prospect that WASH is involved in scission events at endosomes. It is possible that residual WASH during siRNA-mediated suppression led to partial defects, owing to the previously described tubular phenotype. One could envision a scenario in which WASH-mediated F-actin plays a stepwise role in initial tubule initiation, as well as in scission events during the sorting process. For example, WASH could initiate the formation of nascent membrane tubules via subtle F-actin–dependent effects on membrane curvature in order to favor recruitment of BAR domain–containing SNX proteins (van Weering *et al.*, 2010), which would then coat and deform the membrane to create tubules. In the case of siWASH, perhaps residual WASH is actively engaged in the process of tubule initiation, and without additional WASH molecules available for the subsequent actin-dependent scission processes, elongated tubules stretch out from endosomes. However, it must be noted that we were unable to reconcile the effects of siRNA depletion of WASH and tubule formation with the knockout data presented here, even when cells were analyzed shortly after tamoxifen treatment when residual WASH levels remained. Although it is possible that WASH is required for endosomal tubule initiation, possibly in cooperation with BAR-containing proteins (Suetsugu and Gautreau, 2012), the fact that we observed what seemed to be small sorting tubules extending from WASHout endosomes suggests that at least some tubulation was occurring at endosomes independent of WASH.

Alternatively, it is possible that WASH-complex members play unique roles in endosomal processes, such as tubulation, independent of WASH. The fact that there is residual FAM21 and SWIP (and likely strumpellin) that is localized to endosomes in the absence of WASH suggests that these SHRC components could have WASH-independent functions. When we transiently suppressed WASH with siRNA, we did not observe such efficient destabilization of SHRC components as we did in WASHout MEFs (Gomez and Billadeau, 2009), suggesting that increased severity of the WASHout phenotype could partly be attributed to dramatic reduction of all SHRC components upon WASH knockout. It will be interesting in the future to investigate potential WASH-independent roles for these SHRC components.

Even though WASHout endosomes were enlarged and collapsed, global mixing of endosomal subcompartments did not occur. There was clear separation between retromer CSC-associated factors and EEA1. This suggests that segregation of these domains is not dependent on WASH-mediated endosomal F-actin. These domains are defined by recruitment of lipid-associated factors, which is dictated by membrane composition. Therefore it seems that separation of the lipid intermediates that define these endosomal subdomains is maintained. However, since the morphology and size of endosomes is altered without WASH, it is hard to interpret what is aberrant and what is normal in regard to the architecture of collapsed WASHout endosomes. It remains possible that endosomal subdomain organization is unchanged in WASHout cells but is just more obvious due to the collapsed phenotype. Thus interpreting the significance of these segregated domains is difficult within this complex system. Nevertheless, we can conclude that loss of the endosomal F-actin network does not induce global compartment fusion since we can observe distinct endosomal domains rich in retromer CSC-associated proteins, EEA1, or TfnR.

Of interest, we did not observe retromer-associated SNX1 and SNX6 strongly localized to the VPS35-rich subdomain of WASHout endosomes. This could indicate that these proteins normally maintain some level of separation from the CSC components as previously suggested (van Weering *et al.*, 2012), which becomes even more apparent upon endosomal collapse. Alternatively, it could indicate a defect in SNX association with retromer CSC-rich domains in WASHout MEFs or that WASH interaction with these factors is important for their recruitment (Gomez and Billadeau, 2009). However, considering that SNX proteins contain two lipid-binding domains—a PX domain for targeting to specific endocytic subcompartments and a BAR domain that might recognize membranes through both curvature and composition (van Weering *et al.*, 2010)—it is plausible that lipid composition defects or shape defects at WASHout endosomes may lead to altered localization. For example, changes of membrane curvature in the absence of WASH-mediated F-actin could cause SNXs by default to localize via PX domains only. In any case, determining the biology that defines this segregation, as well as more in-depth analysis of retromer-associated SNXs (SNX1, 2, 3, 5, 6, and 27) in WASHout MEFs, should yield insight into retromer function (Cullen, 2008; Harterink *et al.*, 2011; Temkin *et al.*, 2011).

We also observed morphological changes in the LAMP1$^+$ lysosomal compartment of WASHout MEFs. Whether enlarged lysosomes arose as an indirect result of F-actin loss within preceding endosomal-related processes or as a direct consequence of WASH activities at lysosomes will require further study. The function of mammalian WASH has been believed to be primarily endosome associated due to its localization pattern (Derivery *et al.*,

2009; Gomez and Billadeau, 2009; Duleh and Welch, 2010). However, partial WASH localization to the MVB/late endosomal and lysosomal compartment has been described (Derivery *et al.*, 2009; Zech *et al.*, 2011), and *Dictyostelium* WASH has a role in lysosomal neutralization (Carnell *et al.*, 2011). We also observed a steady-state relationship of VPS35/WASH complex–rich puncta with some LAMP1$^+$ lysosomes in control cells. In addition, retromer CSC depletion resulted in lysosomal enlargement (Arighi *et al.*, 2004), supporting the role of the retromer in recruitment of the WASH complex (Harbour *et al.*, 2012; Jia *et al.*, 2012). Taken together, these findings suggest that a pool of mammalian WASH could function directly at lysosomes.

Intriguingly, we did find elongated tubules extending from WASHout lysosomes. The reason for the existence of these exaggerated lysosomal tubules and the absence of such tubules on endosomes is unclear. We also observed large lysosomal structures forming upon EGF stimulation in WASHout MEFs. Of interest, these structures were dense and resembled autophagosomes. The formation of such structures could be attributed to increased fusion in the absence of F-actin coating of early/late endosomes, subsequently leading to lysosome swelling. However, regardless of morphological changes, this compartment was functional since ligand-bound EGFR was degraded efficiently. It will be interesting in the future to analyze the role of WASH (and F-actin) in tightly regulated lysosomal-related processes, such as autophagy.

It was unclear whether TfnR recycling was a WASH-regulated process, based on previous studies (Derivery *et al.*, 2009; Duleh and Welch, 2010; Zech *et al.*, 2011). We found that although TfnR accumulated with collapsed endosomes in WASHout MEFs, there was efficient TfnR recycling to the cell surface. Of interest, a recent study showed that α5β1 integrin displayed similar perinuclear accumulation in WASH-suppressed ovarian cells but was instead colocalized within the MVB/late endosomal compartment (Zech *et al.*, 2011). However, α5β1 integrin exhibited a strong recycling defect, perhaps due to the fact that it traffics via a more selective WASH-dependent route than TfnR (Zech *et al.*, 2011). In fact, recent studies suggested that receptors are differentially sorted through either actin-independent bulk recycling processes or through more selective sequence-based slow recycling (Puthenveedu *et al.*, 2010). In this regard, WASH was shown to localize to β2-adrenergic receptor–recycling tubules (Puthenveedu *et al.*, 2010), and its sorting to the cell surface was retromer dependent (and likely WASH complex dependent; Temkin *et al.*, 2011). Thus our data are in agreement with the notion that cargos using a more selective route may have a stronger requirement for WASH.

Although EGFR exhibits minimal recycling after ligand-dependent activation and is primarily sent to the lysosomal pathway, ligand-free receptors can recycle to the cell surface (Sorkin and von Zastrow, 2002). In WASHout MEFs, steady-state EGFR was directed to collapsed lysosomes and degraded. Thus it is likely that basal recycling of EGFR is lost in the absence of WASH, leading to its degradation in the lysosome. Our data indicate that EGFR sorting from the early/late endosome is WASH dependent. However, it is also possible that since we observed enlarged lysosomes in proximity to the collapsed endosomal network, steady-state loss of EGFR might arise from defects related to augmented, proximity-based lysosomal entry. Alternatively, Insall and colleagues suggested that growth factor receptors, which bind F-actin (den Hartigh *et al.*, 1992), might be sorted via direct actin-mediated sorting processes (Carnell *et al.*, 2011). Although the mechanism for differential loss of EGFR is not yet clear, these results are consistent with the idea that distinct receptors differentially traffic via WASH-dependent and WASH-independent mechanisms.

We demonstrated that WASH knockout leads to both morphological and functional changes within the endosomal and lysosomal networks of mammalian cells, contributing to a subset of receptor-trafficking defects. Future studies aimed at understanding the roles that WASH-mediated receptor-trafficking plays at the organismal level using WASH conditional knockout mice, and the continued use of WASHout MEFs to define cellular roles of WASH, will no doubt shed light on the biology surrounding the complex mammalian sorting/recycling network.

MATERIALS AND METHODS

Reagents and antibodies

Reagents were from Sigma-Aldrich (St. Louis, MO) unless specified. We used anti-CAPZ∝, anti-HRS (M-79), anti-SNX6 (H-40), anti-EGFR, and goat anti-EEA1 (N-19) from Santa Cruz Biotechnology (Santa Cruz, CA). Rabbit antibodies against EEA1, APPL1, and Rab7 were from Cell Signaling Technology (Beverly, MA). We also used anti–clathrin heavy chain (Calbiochem, La Jolla, CA), anti–transferrin receptor (Invitrogen, Carlsbad, CA), anti-ARPC2 (Millipore, Billerica, CA), anti-GFP (Roche, Indianapolis, IN), and goat anti-VPS35 (Abcam, Cambridge, MA). Anti-LAMP1 (1D4B) and anti-GM130 were from BD Biosciences (San Diego, CA). Anti-TBC1D5, anti-SNX1, and anti-RUFY1 were from Proteintech Group (Chicago, IL). Antibodies against TGN46 and α-tubulin (DM1A) were from Sigma-Aldrich. Anti-FAM21 was previously described (Gomez and Billadeau, 2009). Anti-CCDC53, anti-strumpellin, and anti-SWIP were also described (Jia *et al.*, 2010). Anti-VPS35 and anti-mWASH were generated by immunizing rabbits with glutathione *S*-transferase fusion proteins containing amino acids 461 to the end of hVPS35 or amino acids 317 to the end of mWASH, respectively (Cocalico Biologicals, Reamstown, PA). Antibodies against ERK, pERK (T202/Y204), cRAF, p-cRAF (S338), JNK, and pJNK (T183/Y185) were from Cell Signaling Technology. For immunofluorescence, conjugated secondary antibodies, rhodamine–phalloidin, Alexa Fluor–transferrin conjugates, and rhodamine-hEGF were from Invitrogen. For flow cytometry, we used anti–transferrin receptor-PE and anti–hEGFR-PE from BD Biosciences and goat anti-EGFR (Sigma-Aldrich), which was labeled with a Dylight-488 Microscale Labeling Kit (Thermo Scientific, Waltham, MA). Human and mouse EGF used for stimulations was from R&D systems (Minneapolis, MN). Bafilomycin A was obtained from LC Laboratories (Woburn, MA).

Generation of *WASH* conditional knockout fibroblasts

Generation of conditional *WASH*-knockout mice and isolation of MEF lines were achieved in collaboration with the Transgenic and Gene Targeted Mouse Shared Resource at the Mayo Clinic (Rochester, MN), using well-established protocols (Dawlaty and van Deursen, 2006). The *WASH*-knockout targeting construct was generated using the previously described pNTKV1901-frt-*lox*P vector system as depicted in Supplemental Figure S1 (Dawlaty and van Deursen, 2006). Protamine-Cre, ER-Cre, and FLPeR mice were obtained from Jackson Laboratory (Bar Harbor, ME). We first bred germline-transmitted mice to FLPeR mice to delete the *Neo* cassette and then crossed the resultant *WASH*$^{+/flox}$ mice with protamine-Cre mice to generate *WASH*$^{-/-}$ animals (not viable). We also bred *WASH*$^{+/flox}$ mice with ER-Cre mice to obtain *WASH*$^{+/flox}$/ER-Cre$^+$ animals, which were crossed with *WASH*$^{+/flox}$ to obtain the appropriate genotypes for MEF isolation (Dawlaty and van Deursen, 2006). MEFs were immortalized using an SV40-expressing retrovirus obtained from Jan van Deursen (Mayo Clinic). ER-Cre$^+$ MEFs were treated with 3 μM 4-OHT as described for *Dyn2/1* deletion (Ferguson *et al.*, 2009). Standard PCR was used to screen for germline transmission

(CATGACTTCTGTGCTCTGTG and GCCGCTCCCGATTCGCAGCGCATCG), floxed *WASH* allele (CGCATTGATCTTCCTATACGC and TGTCAGTCCTATGCTTAGTG), and *Cre* (ACCAGCCAGCTATCAACTCG and TTACATTGGTCCAGCCACC). Experimental procedures involving laboratory mice were reviewed and approved by the Institutional Animal Care and Use Committee of the Mayo Clinic.

Cell culture, stimulation, and immunoblot

Fibroblasts were grown in DMEM medium supplemented with 10% fetal bovine serum and 4 mM L-glutamine. In some cases, MEFs were serum starved for 12 h, stimulated at 37°C using 20 ng/ml mEGF (or hEGF for hEGFR-expressing line) in serum-free media with cyclohexamide (25 µg/mL), washed with phosphate-buffered saline (PBS), and then lysed. For immunoprecipitations (from 500 to 1000 µg of total protein) and whole-cell lysates (from 100 µg), we used NP-40 lysis buffer (25 mM 4-(2-hydroxyethyl)-1-piperazineethanesulfonic acid, pH 7.9, 150 mM NaCl, 1 mM EDTA, 0.5 mM CaCl, 1% NP-40, 1 mM z, 10 µg/ml leupeptin, 5 µg/ml aprotinin, and 1 mM Na_3VO_4) and analyzed experiments by immunoblot as described (Gomez and Billadeau, 2009). Densitometric quantification of Western blots was performed with ImageJ software (National Institutes of Health, Bethesda, MD)

Generation of hEGFR- and mWASH-expressing MEF lines

For generation of the stable hEGFR-GFP–expressing fibroblasts, *WASH* flox/flox fibroblasts were transduced using pBABE retroviral vector system and GP2 packaging line from Clontech (Mountain View, CA) using the manufacturer's protocol. WASHout MEFs stably reconstituted with GFP-mWASH wild type and ΔVCA were generated using the same system.

Immunofluorescence

MEFs were grown directly on coverslips at 37°C and then fixed immediately in 4% paraformaldehyde without prior PBS washing. The coverslips were then prepared for immunofluorescence as described (Gomez and Billadeau, 2009). For imaging transferrin-labeled cells, MEFs were serum starved for 1 h and then incubated with 10 µg/ml AF555-Tfn for 30 min at 37°C in internalization media (DMEM + 0.5% bovine serum albumin [BSA]). Images were obtained with an LSM-710 laser scanning confocal microscope using Zen software (Carl Zeiss, Jena, Germany). Codistributions of markers in fluorescence images were quantified using colocalization coefficients generated by Zen software (Carl Zeiss), which assigns a numerical value between 0 and 1 (0 = no colocalization; 1 = complete colocalization). In some cases, the intensity was increased when imaging WASHout EGFR-GFP cells compared with control cells in order to efficiently visualize localization of reduced EGFR levels.

Flow cytometry and transferrin uptake/recycling

For flow cytometry, fibroblasts were lifted using Cell Dissociation Solution (Sigma-Aldrich) and then incubated with anti–TfnR-PE (1:200), anti–hEGFR-PE (1:10), or anti–EGFR-DL488 (5 µg/ml) in fluorescence-activated cell sorting (FACS) buffer (PBS with 0.5% BSA) for up to 1 h on ice, washed in ice-cold FACS buffer, and analyzed. For transferrin uptake, MEFs were serum starved for 1 h in DMEM, incubated in prewarmed internalization media containing AF488-Tfn (10 µg/ml) as indicated, washed once in prewarmed DMEM, lifted using Cell Dissociation Solution, instantly fixed in ice-cold paraformaldehyde (1% final concentration), and analyzed by flow cytometry. Transferrin recycling was measured by removing AF488-Tfn–containing media after 30 min of uptake, washing the cells with prewarmed DMEM, and adding internalization media containing AF647-Tfn (10 µg/ml). Cells were then harvested as described and analyzed by two-color flow cytometry as indicated. All flow cytometry was conducted using a FACSCanto II with FACSDiva software (BD Biosciences).

RNA extraction and quantitative reverse transcriptase PCR

Quantitative analysis of mRNA expression was done as described (Zhang *et al.*, 2011). Briefly, RNA was isolated from mouse fibroblasts using the RNeasy Mini Kit (Qiagen, Valencia, CA), and 1 µg of total RNA was reverse transcribed into cDNA using the Superscript III RT-PCR Kit according to the manufacturer's instructions (Invitrogen). Quantitative reverse transcriptase PCR was performed using the comparative CT method with SYBR Green PCR Master Mix and the ABI Prism 7900TM Sequence Detection System (Applied Biosystems, Foster City, CA). Experiments were performed in triplicate, using independent cDNAs. Gene-specific primers were designed using software from the Integrated DNA Technologies website (http://www.idtdna.com). Sequences are as follows: mouse RPLP0 5′-AGATCCGCATGTCCCTTC-3′ and 5′-CCTTGCGCATCATGGTGTT-3′ and mouse EGFR 5′-GGAGGAAAAGAAAGTCTGCC-3′ and 5′-ATCGCACAGCACCAATCAGG-3′.

ACKNOWLEDGMENTS

We thank members of the Billadeau laboratory, Michael Rosen, Da Jia, and Ryan Potts (UT Southwestern Medical Center, Dallas, TX), and Janis K. Burkhardt (University of Pennsylvania, Philadelphia, PA) for helpful discussions. We also thank Jan van Deursen for help with generation of the WASHout construct and Karthikbabu Jeganathan for help with MEF isolation (Mayo Clinic). This work was supported by the Mayo Foundation and National Institutes of Health Grant R01-AI065474 (D.D.B.) and Allergic Diseases Training Grant NIH-T32-AI07047 (T.S.G.). D.D.B. is a Leukemia and Lymphoma Society Scholar.

REFERENCES

Arighi CN, Hartnell LM, Aguilar RC, Haft CR, Bonifacino JS (2004). Role of the mammalian retromer in sorting of the cation-independent mannose 6-phosphate receptor. J Cell Biol 165, 123–133.

Carnell M, Zech T, Calaminus SD, Ura S, Hagedorn M, Johnston SA, May RC, Soldati T, Machesky LM, Insall RH (2011). Actin polymerization driven by WASH causes V-ATPase retrieval and vesicle neutralization before exocytosis. J Cell Biol 193, 831–839.

Chen Z, Borek D, Padrick SB, Gomez TS, Metlagel Z, Ismail AM, Umetani J, Billadeau DD, Otwinowski Z, Rosen MK (2010). Structure and control of the actin regulatory WAVE complex. Nature 468, 533–538.

Cullen PJ (2008). Endosomal sorting and signalling: an emerging role for sorting nexins. Nat Rev Mol Cell Biol 9, 574–582.

Dawlaty MM, van Deursen JM (2006). Gene targeting methods for studying nuclear transport factors in mice. Methods 39, 370–378.

den Hartigh JC, van Bergen en Henegouwen PM, Verkleij AJ, Boonstra J (1992). The EGF receptor is an actin-binding protein. J Cell Biol 119, 349–355.

Derivery E, Sousa C, Gautier JJ, Lombard B, Loew D, Gautreau A (2009). The Arp2/3 activator WASH controls the fission of endosomes through a large multiprotein complex. Dev Cell 17, 712–723.

Duleh SN, Welch MD (2010). WASH and the Arp2/3 complex regulate endosome shape and trafficking. Cytoskeleton (Hoboken) 67, 193–206.

Ferguson SM *et al.* (2009). Coordinated actions of actin and BAR proteins upstream of dynamin at endocytic clathrin-coated pits. Dev Cell 17, 811–822.

Goley ED, Welch MD (2006). The ARP2/3 complex: an actin nucleator comes of age. Nat Rev Mol Cell Biol 7, 713–726.

Gomez TS, Billadeau DD (2009). A FAM21-containing WASH complex regulates retromer-dependent sorting. Dev Cell 17, 699–711.

Harbour ME, Breusegem SY, Antrobus R, Freeman C, Reid E, Seaman MNJ (2010). The cargo-selective retromer complex is a recruiting hub for protein complexes that regulate endosomal tubule dynamics. J Cell Sci 123, 3703–3717.

Harbour ME, Breusegem SY, Seaman MNJ (2012). Recruitment of the endosomal WASH complex is mediated by the extended "tail" of Fam21 binding to the retromer protein Vps35. Biochem J 442, 209–220.
Harterink M *et al*. (2011). A SNX3-dependent retromer pathway mediates retrograde transport of the Wnt sorting receptor Wntless and is required for Wnt secretion. Nat Cell Biol 13, 914–923.
Hernandez-Valladares M, Kim T, Kannan B, Tung A, Aguda AH, Larsson M, Cooper JA, Robinson RC (2010). Structural characterization of a capping protein interaction motif defines a family of actin filament regulators. Nat Struct Mol Biol 17, 497–503.
Jia D, Gomez TS, Billadeau DD, Rosen MK (2012). Multiple repeat elements within the FAM21 tail link the WASH actin regulatory complex to the retromer. Mol Biol Cell 23, 2352–2356.
Jia D, Gomez TS, Metlagel Z, Umetani J, Otwinowski Z, Rosen MK, Billadeau DD (2010). WASH and WAVE actin regulators of the Wiskott-Aldrich syndrome protein (WASP) family are controlled by analogous structurally related complexes. Proc Natl Acad Sci USA 107, 10442–10447.
Linardopoulou EV, Parghi SS, Friedman C, Osborn GE, Parkhurst SM, Trask BJ (2007). Human subtelomeric WASH genes encode a new subclass of the WASP family. PLoS Genet 3, e237.
Puthenveedu MA, Lauffer B, Temkin P, Vistein R, Carlton P, Thorn K, Taunton J, Weiner OD, Parton RG, von Zastrow M (2010). Sequence-dependent sorting of recycling proteins by actin-stabilized endosomal microdomains. Cell 143, 761–773.
Raiborg C, Bache KG, Gillooly DJ, Madshus IH, Stang E, Stenmark H (2002). Hrs sorts ubiquitinated proteins into clathrin-coated microdomains of early endosomes. Nat Cell Biol 4, 394–398.
Raiborg C, Bache KG, Mehlum A, Stang E, Stenmark H (2001). Hrs recruits clathrin to early endosomes. EMBO J 20, 5008–5021.
Rottner K, Hänisch J, Campellone KG (2010). WASH, WHAMM and JMY: regulation of Arp2/3 complex and beyond. Trends Cell Biol 20, 650–661.
Sorkin A, von Zastrow M (2002). Signal transduction and endocytosis: close encounters of many kinds. Nat Rev Mol Cell Biol 3, 600–614.
Suetsugu S, Gautreau A (2012). Synergistic BAR-NPF interactions in actin-driven membrane remodeling. Trends Cell Biol 22, 141–150.
Takenawa T, Suetsugu S (2007). The WASP-WAVE protein network: connecting the membrane to the cytoskeleton. Nat Rev Mol Cell Biol 8, 37–48.
Temkin P, Lauffer B, Jäger S, Cimermancic P, Krogan NJ, von Zastrow M (2011). SNX27 mediates retromer tubule entry and endosome-to-plasma membrane trafficking of signalling receptors. Nat Cell Biol 13, 715–721.
van Weering JRT, Verkade P, Cullen PJ (2010). SNX-BAR proteins in phosphoinositide-mediated, tubular-based endosomal sorting. Semin Cell Dev Biol 21, 371–380.
van Weering JRT, Verkade P, Cullen PJ (2012). SNX-BAR-mediated endosome tubulation is co-ordinated with endosome maturation. Traffic 13, 94–107.
Yamamoto H, Koga H, Katoh Y, Takahashi S, Nakayama K, Shin H-W (2010). Functional cross-talk between Rab14 and Rab4 through a dual effector, RUFY1/Rabip4. Mol Biol Cell 21, 2746–2755.
Zech T, Calaminus SDJ, Caswell P, Spence HJ, Carnell M, Insall RH, Norman J, Machesky LM (2011). The Arp2/3 activator WASH regulates 51-integrin-mediated invasive migration. J Cell Sci 124, 3753–3759.
Zhang J-S, Koenig A, Harrison A, Ugolkov AV, Fernandez-Zapico ME, Couch FJ, Billadeau DD (2011). Mutant K-Ras increases GSK-3β gene expression via an ETS-p300 transcriptional complex in pancreatic cancer. Oncogene 30, 3705–3715.
Zoncu R, Perera RM, Balkin DM, Pirruccello M, Toomre D, De Camilli P (2009). A phosphoinositide switch controls the maturation and signaling properties of APPL endosomes. Cell 136, 1110–1121.